Resting-state Network-specific Breakdown of Functional Connectivity during Ketamine Alteration of Consciousness in Volunteers

Vincent Bonhomme, M.D., Ph.D., Audrey Vanhaudenhuyse, Ph.D., Athena Demertzi, Ph.D., Marie-Aurélie Bruno, Ph.D., Oceane Jaquet, M.D., Mohamed Ali Bahri, Ph.D., Alain Plenevaux, Ph.D., Melanie Boly, M.D., Ph.D., Pierre Boveroux, M.D., Ph.D., Andrea Soddu, Ph.D., Jean François Brichant, M.D., Ph.D., Pierre Maquet, M.D., Ph.D., Steven Laureys, M.D., Ph.D.

ABSTRACT

Background: Consciousness-altering anesthetic agents disturb connectivity between brain regions composing the resting-state consciousness networks (RSNs). The default mode network (DMn), executive control network, salience network (SALn), auditory network, sensorimotor network (SMn), and visual network sustain mentation. Ketamine modifies consciousness differently from other agents, producing psychedelic dreaming and no apparent interaction with the environment. The authors used functional magnetic resonance imaging to explore ketamine-induced changes in RSNs connectivity.

Methods: Fourteen healthy volunteers received stepwise intravenous infusions of ketamine up to loss of responsiveness. Because of agitation, data from six subjects were excluded from analysis. RSNs connectivity was compared between absence of ketamine (wake state [W1]), light ketamine sedation, and ketamine-induced unresponsiveness (deep sedation [S2]).

Results: Increasing the depth of ketamine sedation from W1 to S2 altered DMn and SALn connectivity and suppressed the anticorrelated activity between DMn and other brain regions. During S2, DMn connectivity, particularly between the medial prefrontal cortex and the remaining network (effect size β [95% CI]: W1 = 0.20 [0.18 to 0.22]; S2 = 0.07 [0.04 to 0.09]), and DMn anticorrelated activity (*e.g.*, right sensory cortex: W1 = −0.07 [−0.09 to −0.04]; S2 = 0.04 [0.01 to 0.06]) were broken down. SALn connectivity was nonuniformly suppressed (*e.g.*, left parietal operculum: W1 = 0.08 [0.06 to 0.09]; S2 = 0.05 [0.02 to 0.07]). Executive control networks, auditory network, SMn, and visual network were minimally affected.

Conclusions: Ketamine induces specific changes in connectivity within and between RSNs. Breakdown of frontoparietal DMn connectivity and DMn anticorrelation and sensory and SMn connectivity preservation are common to ketamine and propofol-induced alterations of consciousness. **(Anesthesiology 2016; 125:873-88)**

ANESTHESIA-INDUCED alteration of consciousness involves complex disturbances of communication between brain regions or functional connectivity.[1] Functional magnetic resonance imaging (fMRI) can demonstrate such effects of anesthesia.[2] Functional connectivity as evidenced by fMRI corresponds to statistical dependencies in changes of an indirect sign of regional brain activity,[3] the blood oxygen level–dependent (BOLD) signal fluctuation, which quantifies regional cerebral blood flow (CBF).

Among anesthetic agents with hypnotic properties, those targeting γ-aminobutyric acid–mediated (GABA)ergic neurotransmission have been studied the most with respect to their effect on brain connectivity. Among them, propofol induces complex changes into specific networks,[4] possibly through reconfiguration of their topology.[5] In addition to disrupting frontal-parietal connectivity[6–8] and inhibiting

What We Already Know about This Topic

- General anesthetics disrupt functional connectivity between various brain regions as assessed by functional magnetic resonance imaging.
- Ketamine has distinct pharmacologic and electrophysiologic effects compared to other general anesthetics.

What This Article Tells Us That Is New

- In human volunteers, ketamine alters connectivity within and between resting-state consciousness networks, notably by disrupting frontoparietal connectivity while sensory and sensorimotor networks are preserved.
- While ketamine has certain distinct effects on connectivity within and between resting-state consciousness networks, its functional disruption of frontoparietal cortical communication is shared by several other general anesthetics with distinct pharmacologic profiles.

This article is featured in "This Month in Anesthesiology," page 1A. Corresponding article on page 830. Supplemental Digital Content is available for this article. Direct URL citations appear in the printed text and are available in both the HTML and PDF versions of this article. Links to the digital files are provided in the HTML text of this article on the Journal's Web site (www.anesthesiology.org). V.B. and A.V. equally contributed to this article.

Submitted for publication November 12, 2015. Accepted for publication June 8, 2016. From the University Department of Anesthesia and Intensive Care Medicine, CHR Citadelle and CHU University Hospital of Liege, Liege, Belgium (V.B., O.J.); Coma Science Group, GIGA Research, University and CHU University Hospital of Liege, Liege, Belgium (V.B., A.V., A.D., M.-A.B., M.A.B., S.L.); GIGA-Cyclotron Research Center:

 Anesthesiology 2016; 125:873-88

<zdoi;10.1097/ALN.0000000000001275>

nonspecific thalamocortical connectivity involved in cortical arousal,[4,9] propofol is known to affect functional brain networks that are essential to the emergence of a mental content.[10] Those networks are qualified as resting-state consciousness networks (RSNs) because of being active in resting task-free individuals. RSNs affected by propofol include the default mode network (DMn) involved in the awareness of self, autobiographical memory, mind wandering, and unconstrained cognition[11]; the left and right executive control networks (LECn and RECn) involved in perceptual, somesthetic processing, ability to respond to an external event, and to have conscious reportable perception[12,13]; and the salience network (SALn) involved in judgment of an event salience, conflict monitoring, information integration, response selection, interoceptive processes, and the emotional counterpart of pain.[4,14] At doses of propofol that produce unresponsiveness to verbal command, the thalamocortical connectivity specific to those networks is preserved,[15] as well as connectivity in sensory networks,[10] while interactions between sensory modes, such as the auditory or visual modes, are altered. Coordination of activity between consciousness networks is also impeded by propofol, insofar as it phases out the activity alternation between DMn and executive control network (ECn).[10,16]

Ketamine has hypnotic properties, but is rather different from GABAergic agents. Increasing concentrations first produce antidepression, followed by analgesia and psychotomimesis, including feelings of dissociation, hallucinations, and delirium. Loss of responsiveness occurs only at the highest doses.[17] The molecular targets of propofol and ketamine are distinct; in contrast to propofol, the hypnotic effects of ketamine appear to be largely mediated by blockade of *N*-methyl-D-aspartate receptors and hyperpolarization-activated cyclic nucleotide-gated cation type 1 channels.[17]

Short- and long-term modulation of brain connectivity by ketamine has recently been evidenced.[18] Small doses decrease connectivity between DMn and other networks involved in depression pathophysiology.[19] Ketamine analgesia is related to diminished connectivity between sensory networks and regions responsible for pain sensing and affective processing and to increased connectivity with regions involved in the descending inhibition of pain.[20] At plasma concentrations that produce psychotomimesis, ketamine induces global brain hyperconnectivity and reorganization of sensory networks,[20,21] possibly leading to unconstrained cognition. Ketamine also alters the dorsolateral prefrontal cortex connectivity that relates to working memory.[22] Finally, directional frontal-parietal connectivity is impaired in patients receiving doses of ketamine that induce loss of responsiveness.[23,24]

No systematic exploration of the effects of ketamine on consciousness RSNs themselves has been undertaken so far, and very few ketamine connectivity studies have used doses susceptible to produce unresponsiveness to command. Hence, in this fMRI study, we aimed at exploring within and between RSNs' connectivity in healthy volunteers submitted to stepwise increments in ketamine plasma concentration, up to loss of responsiveness to verbal command. Insofar as ketamine and GABAergic agents have different biochemical targets and produce very different anesthetic states, we hypothesized that ketamine would produce a different connectivity pattern.

Subjects and Methods

Subjects

After approval by the Ethics Committee of the Medical School of the University of Liege (University Hospital, Liege, Belgium), study registration (EudraCT 2010-023016-13), and obtaining informed consent by the volunteers to participate in the study, 14 right-handed volunteers were recruited (5 women; median age [range], 25 [19 to 31] yr; mean body mass index [range], 24 [20 to 31] kg/m^2). Among them, six in total had to be excluded from the study and further data analysis because of excessive agitation and movements (five subjects) or voluntary withdrawal (one subject). The volunteers were recruited through advertisement in an Internet forum and underwent medical interview and physical examination before their participation. Exclusion criteria for recruitment included inappropriate contraception for women, history of head trauma or surgery, mental illness, drug addiction, asthma, motion sickness, previous problems during anesthesia, or any of the classical contraindications for an MRI examination, such as vascular clips or metallic implants, and claustrophobia. All volunteers received financial compensation for inconvenience and time lost during the experiment.

Experimental Design, Equipment, and Infusion of Ketamine

The volunteers were requested to fast for at least 6 h from solids and 2 h from liquids before the experimental session. Once in the investigation unit, a systematic review of eventual contraindications to participation was again performed, including criteria for both anesthesia and MRI, using a detailed checklist. Thereafter, an MRI structural image acquisition occurred (see the first paragraph of Functional Data Acquisition, Extraction of Resting-state Networks, and Group Analysis).

After structural image acquisition, subjects were removed from the MRI scanner, and 64 electroencephalogram (EEG) scalp electrodes were placed to allow for simultaneous EEG

In Vivo Imaging, University of Liege, Liege, Belgium (A.V., A.D., M.-A.B., M.A.B., A.P., A.S., P.M., S.L.); Departments of Algology and Palliative Care (A.V.), Anesthesia and Intensive Care Medicine (V.B., O.J., P.B., J.F.B.), and Neurology (P.M., S.L.), CHU University Hospital of Liege, Liege, Belgium; Department of Neurology, University of Wisconsin, Madison, Wisconsin (M.B.); Departments of Anesthesia and Intensive Care Medicine (P.B.); Department of Physics and Astronomy, The University of Western Ontario, London, Ontario, Canada (A.S.); and Institut du Cerveau et de la Moelle épinière – ICM, Hôpital Pitié-Salpêtrière, Paris, France (A.D.).

recording during fMRI data acquisition (Brain Amp® magnetic resonance compatible acquisition setup; Brain Products GmbH, Germany). In this report, data analysis, however, has been restricted to fMRI data only.

An 18-gauge intravenous catheter (BD Insyte-W; Becton Dickinson Infusion Therapy Systems Inc., USA) was then placed into a vein of the left forearm and infused using normal saline at a rate of 20 ml/h. The intravenous line served for ketamine infusion and eventual administration of rescue medications. A 20-gauge arterial catheter (Arrow® International Inc., USA) was also placed into the left radial artery, under strict sterile conditions and after performing local anesthesia with 3 ml of 1% lidocaine. This catheter was equipped with a monitoring set (TruWave, Edwards Lifesciences, Dominican Republic) and served for arterial blood sampling and gas analysis. Standard MRI-compatible anesthesia monitoring (Magnitude 3150M; Invivo Research, Inc., USA) was also placed to allow continuous monitoring and recording of the electrocardiogram, heart rate, blood pressure, pulse oxymetry (Spo_2), and breathing frequency throughout the scanning and recovery periods. Through a loosely fitting plastic facemask, additional oxygen at a rate of 5 l/min was provided to volunteers, whose breathing always remained spontaneous. One certified anesthesiologist and one neurologist were present throughout the experiment. In case of trouble, complete resuscitation equipment and medications were immediately available at the door side of the MRI scanner.

After setting all needed equipment and monitoring, the volunteers were comfortably installed in the MRI tray. The most comfortable supine position attainable was sought to avoid painful stimulation related to position. All volunteers wore earplugs to attenuate noise and earphones to allow communication with investigators; one investigator remained in the MRI scan room at all times.

Ketamine was administered using a computer-controlled intravenous infusion device composed of a separate laptop computer. The computer was running the StanPump software (S. L. Shafer, Perioperative and Pain Medicine, Stanford University, Stanford, California; East Bay Anesthesiology Medical Group, Alta Bates Summit Medical Center, Oakland, California) and was connected to an infusion pump (Graseby 3400, Smith Medical International Ltd, United Kingdom) through a serial port. A 50-ml syringe was filled with normal saline containing racemic ketamine (Ketalar, Pfizer Ltd., Turkey) at a concentration of 10 mg/ml. The pharmacokinetic model used to drive the pump was the Domino model,[25] which has been demonstrated to have acceptable predictive performance.[26] This system commands infusion pump rates to allow targeting precise effect-site and plasma concentrations of ketamine, based on several biometric parameters. For each change in ketamine concentration, a 5-min equilibration period was allowed after reaching the target, to permit equilibration of ketamine concentration between body compartments.

The depth of sedation was assessed using the Ramsay scale (RS: 1 = anxious, agitated, or both; 2 = cooperative, oriented, and calm; 3 = response to command only, clear but slow; 4 = evident response to glabellum stimulation or to loud auditory stimulation; 5 = slow response to glabellum stimulation or to loud auditory stimulation; and 6 = no response)[27] and the University of Michigan Sedation Scale (UMSS: 0 = awake and alert; 1 = lightly sedated, tired, appropriate response to conversation and/or to sounds; 2 = moderate sedation, drowsy, easily aroused by tactile stimulation; 3 = deep sedation, deep sleep, aroused only by strong physical stimulation; and 4 = impossible to arouse).[28] Each evaluation took place immediately before and after each fMRI data acquisition sequence. Volunteers were asked to strongly squeeze the hand of the investigator, and the command was repeated twice. For that purpose, and for close watch of the volunteer, an investigator continuously stayed inside the MRI room.

The procedure of data acquisition is illustrated in figure 1. After equipment and monitoring placement, as well as comfortable volunteer installation onto the MRI scan tray, a first fMRI data acquisition was performed in the absence of any infusion of ketamine (baseline recording = wake state [W1]). Data acquisition was always preceded and followed by the depth of sedation assessment and arterial blood sampling. Ketamine infusion was then started, and its target concentration was increased by steps of 0.5 μg/ml until a level of sedation corresponding to RS 3 to 4 or UMSS 1 to 2 was reached (light sedation, S1). After the 5-min equilibration period, a novel sequence of data acquisition occurred, consisting of the same sequence of events as during W1. Ketamine target concentration was then further increased by steps of 0.5 μg/ml until RS 5 to 6 or UMSS 4 (deep sedation [S2]), and the same sequence of data acquisition was again performed. After those acquisitions, the infusion of ketamine was stopped, and the subject was removed from the fMRI scanner to allow for comfortable recovery. Because of frequent nausea, all volunteers preventively received 50 mg of alizapride and 4 mg of ondansetron intravenously immediately after the end of ketamine infusion. Throughout the acquisition sequence and the recovery period, hemodynamic, EEG, and oxygenation parameters were continuously monitored (vital parameters). Volunteers were discharged from the investigation unit only when having fully recovered and duly accompanied. They were given a phone number to call in case of problem and were contacted by phone the day after to check whether they had been able to recover normal activity that day.

The presence of dreaming during ketamine infusion was checked through a phone call at distance from the experimental session. A detailed description of dream themes was recorded.

Functional Data Acquisition, Extraction of Resting-state Networks, and Group Analysis

Resting-state fMRI volume acquisition occurred during normal wakefulness (W1, RS 2, UMSS 0), S1 (RS 3 to 4,

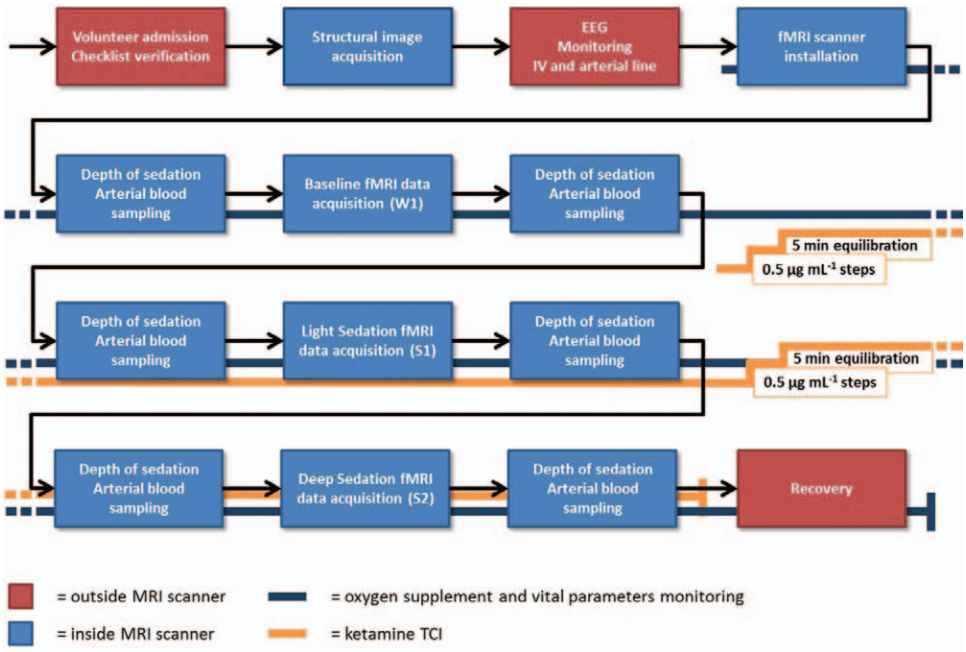

Fig. 1. Time line of data acquisition. Depth of sedation = depth of sedation assessment using Ramsay Scale and University of Michigan Sedation Scale; electroencephalogram (EEG) = installation of EEG electrodes; fMRI = functional magnetic resonance imaging; monitoring = hemodynamic and oxygenation (vital parameters) monitoring placement; S1 = light sedation condition, corresponding to a Ramsay score (RS) of 3 or 4 and to a University of Michigan Sedation score (UMSS) of 1 or 2; S2 = deep sedation condition, corresponding to a RS of 5 or 6 and to a UMSS of 4; TCI = target-controlled infusion; W1 = baseline condition, in the absence of any ketamine infusion; 0.5-µg/ml steps = size of each increase in ketamine target concentration until desired level of sedation attained; 5-min equilibration = 5-min equilibration period after achieving desired target concentration of ketamine and level of sedation.

UMSS 1 to 2), and S2 (RS 5 to 6). Because ketamine has a long elimination half-life and to limit time spent in the fMRI scanner for the volunteer, the temporal order of those clinical states was not randomized. For the same reason, a recovery experimental condition could not be achieved. The number of scans per session was similar among subjects for all three clinical states (mean [SD], 301 [5] scans per session). Data were acquired on a 3T Siemens Allegra scanner (Siemens AG, Germany; Echo Planar Imaging sequence using 32 slices; repetition time = 2,460 ms; echo time = 40 ms; field of view = 220 mm; voxel size = 3.45 × 3.45 × 3 mm; and matrix size = 64 × 64 × 32). A high-resolution structural T1 image was acquired in each volunteer at the beginning of the whole experiment for coregistration to the functional data.

Low-frequency BOLD correlations between brain regions were investigated using a multiple region of interest (ROI)–driven analysis, searching for brain areas correlated to a set of selected seed regions after removal of spurious physiologic noise.[29] This ROI-driven analysis was similar to the one described in our previous article,[10] although with some differences, and consisted of obtaining single-subject connectivity maps before combining them into group-level network maps. The whole analysis included the following steps: realignment, normalization, smoothing, nuisance correction and individual extraction of seed-to-voxel connectivity maps, and multiple seed network and group analysis of modifications across experimental conditions (fig. 1, Supplemental Digital Content 1, http://links.lww.com/ALN/B304).

Functional and structural images were first realigned, normalized, and smoothed (8-mm full width at half maximum) using Statistical Parametric Mapping (SPM) software version 8 (Wellcome Trust Center for Neuroimaging; http://www.fil.ion.ucl.ac.uk/spm/).

Subsequent steps were performed using a functional connectivity toolbox (CONN, version 15.f, MATLAB-based cross-platform software, freely available from NITRC at http://www.nitrc.org/projects/conn/). Extraction of DMn, LECn, RECn, SALn, auditory network (AUDn), sensorimotor network (SMn), and visual network (VISn) consisted in extracting BOLD time courses of interest that were computed as the first principal component of the BOLD signal in 10- or 4-mm radius spherical ROIs centered on *a priori* coordinates reported in previous work. For each network, a set of ROIs known to pertain to the concerned network were chosen, and extraction occurred first for each ROI individually. ROIs are described in table 1, including their x, y, and z Montreal Neurologic Institute coordinates in millimeters, and are identical to those reported in our previously published article.[35] ROIs for the DMn included regions centered in the posterior cingulate cortex/precuneus, the medial prefrontal cortex (MPFC), the left and right lateral parietal

Table 1. Description of Regions of Interest (seeds) Used to Define Each of the Studied Networks

Network	BA	Region	x, y, z	Abbreviation	References
Default mode network	31	Posterior cingulate cortex/precuneus	0 –52 27	PCC-Prec	Raichle[30]
	9	Medial prefrontal cortex	–1 54 27	MPFC	
	39	L/R lateral parietal cortex	–46 –66 30/49 –63 33	LPC/RPC	
	21	L/R inferior temporal cortex	–61 –24 –9/58 –24 –9	LITC/RITC	
		L/R cerebellum	–25 –81 –33/25 –81 –33	LCere/RCere	
		Thalamus*	0 –12 9	Thal	
		Brainstem*	12 –24 –24	BrSt	Boveroux *et al*.[10]
L/R executive control networks	9	L/R dorsolateral prefrontal cortex	–43 22 34/43 22 34	LDLPFC/RDLPFC	Fair *et al*.[31]
	40	L/R inferior parietal lobule	–51 –51 36/51 –47 42	LIPL/RIPL	
	6	L/R premotor cortex	–41 3 36/41 3 36	LPMC/RPMC	
	23	Midcingulate cortex	0 –29 30	MCingC	
	39	L/R angular gyrus	–31 –59 42/30 –61 39	LAG/RAG	
	7	L/R precuneus	–9 –72 37/10 –69 39	LPrec/RPrec	
		Brainstem*	12 –24 –24	BrSt	Boveroux *et al*.[10]
		Cerebellum	–4 –56 –40	Cere	
		L/R thalamus*	–4 –12 0/4 –12 0	LThal/RThal	
Salience network	12	Orbital frontoinsula	–40 18 –12/42 10 –12	LOFI/ROFI	Seeley *et al*.[32]
	38	L/R temporal pole	–52 16 –14/52 20 –18	LTP/RTP	
	32	Paracingulate	0 44 28	ParaCing	
	24	L/R dorsal anterior cingulate	–6 18 30/6 22 30	LDACing/RDACing	
	6	L/R supplementary motor area	–4 14 48/4 14 48	LSMA/RSMA	
	22	L/R superior temporal gyrus	–62 –16 8/64 –38 6	LSTG/RSTG	
	40	L/R parietal operculum	–60 –40 40/58 –40 30	LPO/RPO	
	47	Ventrolateral prefrontal cortex	42 46 0	VLPFC	
	46	L/R dorsolateral prefrontal cortex	–38 52 10/30 48 22	LDLPFC-2/ RDLPFC-2	
		L/R thalamus*	–12 –18 6/12 –18 6	LThal-2/RThal-2	
		L/R hypothalamus*	–10 –14 –8/6 –16 –6	LHypo/RHypo	
		Periaqueductal gray*	–4 –24 –2	PAG	
		L/R ventral tegmental area*	8 –8 –14/–10 –14 –10	LVTA/RVTA	
Auditory network	41/42	L/R superior transverse temporal gyrus	–44 –6 11/44 –6 11	LSTTG/RSTTG	Maudoux *et al*.[33]
	6	L/R precentral gyrus	–53 –6 8/58 –6 11	LPCG/RPCG	
	24	Anterior cingulate cortex	6 –7 43	ACingC	
	19	L/R visual cortex	–6 –88 37/6 –88 37	LVC/RVC	
Sensorimotor network	3	L/R primary motor cortex	–39 –26 51/38 –26 48	LPrMC/RPrMC	Raichle[30]
		Supplementary motor area	0 –21 48	SMA	
Visual network	17	L/R primary visual cortex	–13 –85 6/8 –82 6	LPVC/RPVC	De Luca *et al*.[34]
	18	L/R secondary visual cortex	–6 –78 –3/6 –78 –3	LSVC/RSVC	
	19	L/R associative visual cortex	–30 –89 20/30 –89 20	LAVC/RAVC	

The x, y, and z Montreal Neurological Institute peak coordinates are given in millimeter. Literature references to justify the choice of those seed coordinates for defining a network are also provided.

*All seeds were defined as 10- or 4-mm-radius spheres around peak coordinates.

ACingC = anterior cingulate cortex; BA = Brodmann area number; BrSt = brain stem; Cere = cerebellum; L/R = left and right; LAG/RAG = left and right angular gyrus; LAVC/RAVC = left and right associative visual cortices; LCere/RCere = left and right cerebellum; LDACing/RDACing = left and right dorsal anterior cingulate; LDLPFC/RDLPFC = left and right dorsolateral prefrontal cortices; LDLPFC-2/RDLPFC-2 = left and right dorsolateral prefrontal cortices; LHypo/RHypo = left and right hypothalamus; LIPL/RIPL = left and right inferior parietal lobules; LITC/RITC = left and right inferior temporal cortices; LOFI/ROFI = left and right orbital frontoinsula; LPC/RPC = left and right parietal cortices; LPCG/RPCG = left and right precentral gyrus; LPMC/RPMC = left and right premotor cortices; LPO/RPO = left and right parietal operculum; LPrec/RPrec = left and right precuneus; LPrMC/RPrMC = left and right premotor cortices; LPVC/RPVC = left and right primary visual cortices; LSMA/RSMA = left and right supplementary motor areas; LSTG/RSTG = left and right superior temporal gyrus; LSTTG/RSTTG = left and right superior transverse temporal gyrus; LSVC/RSVC = left and right secondary visual cortices; LThal/RThal = left and right thalamus; LThal-2/RThal-2 = left and right thalamus; LTP/RTP = left and right temporal poles; LVC/RVC = left and right visual cortices; LVTA/RVTA = left and right ventral tegmental areas; MCingC = midcingulate cortex; MPFC = medial prefrontal cortex; PAG = periaqueductal gray; ParaCing = paracingulate; PCC-Prec = posterior cingulate – precuneus; SMA = supplementary motor area; Thal = thalamus; VLPFC = ventrolateral prefrontal cortex.

cortices, the left and right inferior temporal cortices, the left and right cerebellum, the thalamus,[30] and the brainstem.[10] For the LECn and RECn, ROIs were centered in the left and right dorsolateral prefrontal cortices (LDLPFC and RDLPFC), the left and right inferior parietal lobules, the left and right premotor cortices, the mid-cingulate cortex, the left and right angular gyrus, the left and right precuneus,[31] the brainstems, the cerebellum (Cere), and the left and right thalamus.[10] SALn was defined by 23 ROIs including the left and right orbital frontoinsula, the left and right temporal poles, the paracingulate, the left and right dorsal anterior cingulate, the left and right supplementary motor areas, the

left and right superior temporal gyrus, the left and right parietal operculum, the ventrolateral prefrontal cortex, the left and right dorsolateral prefrontal cortices 2, the left and right thalamus 2, the left and right hypothalamus, the periaqueductal gray, and the left and right ventral tegmental areas.[32] AUDn included ROIs located in the left and right superior transverse temporal gyrus, left and right precentral gyrus, the anterior cingulate cortex (ACingC), and the left and right visual cortices.[33] SMn involved the left and right primary motor cortices and the supplementary motor areas,[30] while VISn encompassed the left and right primary visual cortices, the left and right secondary visual cortices, and the left and right associative visual cortices.[34]

Before extraction of the first eigenvariate of the time courses of voxels in ROIs, functional data were temporally band-pass filtered using a 0.007- to 0.1-Hz Gaussian temporal filter implemented in Oxford Centre for Functional MRI of the Brain Laboratory Software Library (version 3.2; University of Oxford, Oxford, United Kingdom). Similar time course extractions were performed for two other voxels of interest located in the white matter and the lateral ventricles to estimate the global brain signal changes across time and their derivatives. Those data served as nuisance covariates in the statistical model (white matter and cerebrospinal fluid noise). The movement parameters were also added as nuisance covariates in the design matrix. A separate design matrix was created for each ROI in each of the three sessions in every subject. Serial correlations were then estimated with a restricted maximum likelihood algorithm using an intrinsic autoregressive model during parameter estimation. The effects of interest were tested by linear contrasts, generating statistical parametric T maps in each subject. A contrast image was then computed in each session, identifying voxels significantly correlated to the selected seed region after removal of sources of spurious variance.

Second-level analysis consisted of network and group statistics and was also performed using CONN. Individual summary statistics images were entered into a random-effects model in which subjects were considered random variables. Repeated-measures ANOVAs were performed with the three experimental conditions as factors, namely W1, S1, and S2, as well as defined sets of ROIs for each network. In each set of ROIs, the between-sources contrast was defined as 1/(number of considered ROIs), meaning that, for the DMn, for example, the effect of each of the 10 ROIs was weighted as 0.1. In other words, for each network, the time series from the voxels contained in each seed region were extracted and then averaged together. The resulting averaged time course was estimated by taking account of the time courses of more than one region. The averaged time series were used to estimate whole-brain correlation r maps, which were then converted to normally distributed Fisher z-transformed correlation maps to allow for group-level comparisons. This was performed analogously to our previously reported method.[35] This multiple seed approach was used to overcome the problem of the selection of only one seed region for each network, which in principle can lead to as many overlapping networks as the number of possible selectable seeds. Using more seed ensures proper network characterization in volunteers. The error covariance was not assumed to be independent between regressors, and a correction for nonsphericity was applied. We used two-sided T contrasts to test for significant connectivity effects in all our analyses. After model estimation, a first T contrast searched for areas correlated with each selected set of seed region during W1. Second and third analyses then searched for persistent correlations with the set of seed region during S1 and S2. Other T contrasts looked at significant differences between the three experimental conditions, namely W1 against S1, W1 against S2, and S1 against S2. These last subtraction analyses are not reported here, for the sake of not weighting the article down too much. Finally, a linear two-tailed T contrast was computed for each network, searching for a linear relationship between functional connectivity and the depth of sedation across the three conditions (*i.e.*, W1, S1, and S2: contrast [1, 0.5, −1.5]). All analyses were thresholded at false discovery rate (FDR)–corrected $P < 0.05$ at the whole-brain level, except for the regression analyses, where an uncorrected P value of 0.001 was chosen, and each condition was viewed separately for adjustment.

To identify clusters of voxels significantly correlated with sets of ROIs, we used the REX toolbox in SPM (available free at http://gablab.mit.edu/index.php/news/95-gablab-site/gablab/people/swg). This analysis was performed at a cluster level, with no conjunction mask, no scaling, and using a family-wise error–corrected cluster $P < 0.05$.

A last type of two-sided T contrast was performed to test for significant ROI-to-ROI (or seed-to-seed) connectivity within each network for each experimental condition and thresholded at FDR-corrected $P < 0.05$. Insofar as this seed-to-seed analysis limits the exploration to the preselected seed regions, it was used for illustration purpose only. It served to draw graphical representations of networks in each experimental condition, with seed regions plotted on a canonical axial brain slice. In those graphs, seed regions are linked by lines whose thickness and color vary according to the strength of between-seed connectivity.

Additional Statistical Analyses

Within-subject comparison of mean blood pressure, heart rate, peripheral saturation in oxygen, and arterial carbon dioxide partial pressure across experimental conditions were performed using one-way ANOVA for repeated measures and Tukey honestly significant difference tests for *post hoc* comparisons. For those analyses, a two-tailed $P < 0.05$ was considered statistically significant.

Results

Data were collected between February 7, 2011, and February 28, 2012. These data are full original data and have not been used in other studies, analyses, or publications.

Behavioral Observations, Ketamine Concentrations, Vital Parameters, and Side Effects

As mentioned in the first paragraph of Subjects in Subjects and Methods, complete data sets were obtained in 8 of the 14 volunteers who continued the study protocol sufficiently to be installed inside the MRI scanner. The main reason for withdrawal from the study was excessive agitation into the scanner during the experiment for five volunteers; one volunteer withdrew. During a phone call performed on average 327 days after the experiment (range, 66 to 821 days), all volunteers whose data were included in the analysis reported having experienced strange dreams during ketamine administration. The dream themes experienced during ketamine infusion are summarized in table 1 of Supplemental Digital Content 2 (http://links.lww.com/ALN/B305). Themes included sensations of well-being, joy, and peace, sensations of unearthly environment, flying, perceptions of a bright light, sense of day dreaming, sensation of dissolution in the environment, body distortion, falling sensation, feelings of imprisonment, and the sensation of dying. Unfortunately, it was not possible to know whether those dreams occurred during S1 or S2. Nausea was frequent at the end of the experiment when moving the volunteer. Nausea was easily controlled by the intravenous administration of ondansetron and alizapride. No other side effects or incidents are to be reported, and all volunteers fully recovered normal activities on the day after the experiment.

Ketamine attained estimated plasma concentrations, and recorded vital parameters are reported in table 2. The median ketamine concentration was 0.5 μg/ml during S1 and 2 μg/ml during S2. Repeated-measure ANOVA revealed a dose-dependent increase in heart rate and arterial blood pressure during ketamine administration. Contrarily, arterial carbon dioxide remained unchanged. The depth of sedation as assessed by sedation scores was in the predefined range during all conditions.

Connectivity within the Default Mode Network

During W1, cluster analysis (Supplemental Digital Content 3, http://links.lww.com/ALN/B306) confirmed significant connectivity between regions predefined as pertaining to DMn (fig. 2). In addition, a dorsal extension of the MPFC seed region, up to the premotor cortex, was evidenced, as well as a local spreading of the posterior cingulate cortex/precuneus seed region and extension of left and right inferior temporal cortex along the temporal lobe. Three clusters with significant connectivity but not corresponding to predefined ROIs were also identified. Two of them were small regions located on the borders of the left and right perirhinal, entorhinal, and parahippocampal cortices and one of them was located on the lateral and inferior part of the left prefrontal cortex.

Increasing the depth of ketamine sedation produced a progressive breakdown of connectivity within the DMn that was discreet during S1, with most identified clusters still present, and far more pronounced during S2. At that deepest level of sedation, no significant clusters were evidenced. Correlation analysis revealed a significant relationship between increasing the depth of ketamine sedation and decreasing the connectivity of the MPFC with DMn.

Default Mode Network Anticorrelation

During the W1, DMn also showed anticorrelation with several brain regions (fig. 2). Seven anticorrelated clusters were identified. The first one (cluster 7) was covering parts of the right supramarginal gyrus, somatosensory association cortex, primary and secondary somatosensory cortices, and insular cortex, and the second one (cluster 8) involved the right insular cortex, pars triangularis, premotor cortex, dorsolateral prefrontal cortex, superior temporal gyrus, subcentral area, and primary motor cortex. The third cluster (cluster 9) comprised the right and left premotor cortices, ventral ACingC, and dorsal ACingC. The fourth (cluster 10) encompassed the left supramarginal gyrus, somatosensory association cortex, insular cortex, primary auditory cortex, and the subcentral area. The left insular cortex, premotor cortex, superior temporal gyrus, dorsolateral prefrontal cortex, pars triangularis, and subcentral area composed the fifth cluster (cluster 11).

Table 2. Vital Parameters, Sedation Scores, and Ketamine Concentrations

Parameter	W1	S1	S2	Statistics
Mean blood pressure, mmHg, mean (SD)	94 (11)*	107 (13)†	120 (16)	$F_{(2, 14)} = 19.14$, $P < 0.0001$
Heart rate, beats/min, mean (SD)	70 (14)*	92 (18)†	108 (10)	$F_{(2, 14)} = 27.97$, $P < 0.0001$
Peripheral saturation in oxygen, (%, mean (SD)	99 (0)	99 (0)	98 (1)	$F_{(2, 14)} = 2.70$, NS
Estimated ketamine plasma concentration, μg/ml, median (range)	N/A	0.75 (0.5–1.5)	2 (1.5–2.5)	N/A
Measured arterial carbon dioxide partial pressure, mmHg, mean (SD)	41 (4)	39 (7)	37 (8)	$F_{(2, 14)} = 1.22$, NS
Ramsay sedation score, median (range)	2 (2–2)	2 (2–3)	6 (4–6)	N/A
University of Michigan Sedation Score, median (range)	0 (0–0)	1.5 (0–2)	4 (3–4)	N/A

Parameters are reported for the baseline condition (W1), light sedation (S1), and deep sedation (S2). Results of the one-way ANOVA for repeated measures are further provided (statistics).

*Significantly lower than at S1 and S2 as assessed by Tukey honestly significant difference tests on 3 means with 14 degrees of freedom. †Significantly lower than S2 as assessed by the same *post hoc* comparison tests.

N/A = nonapplicable; NS = nonsignificant.

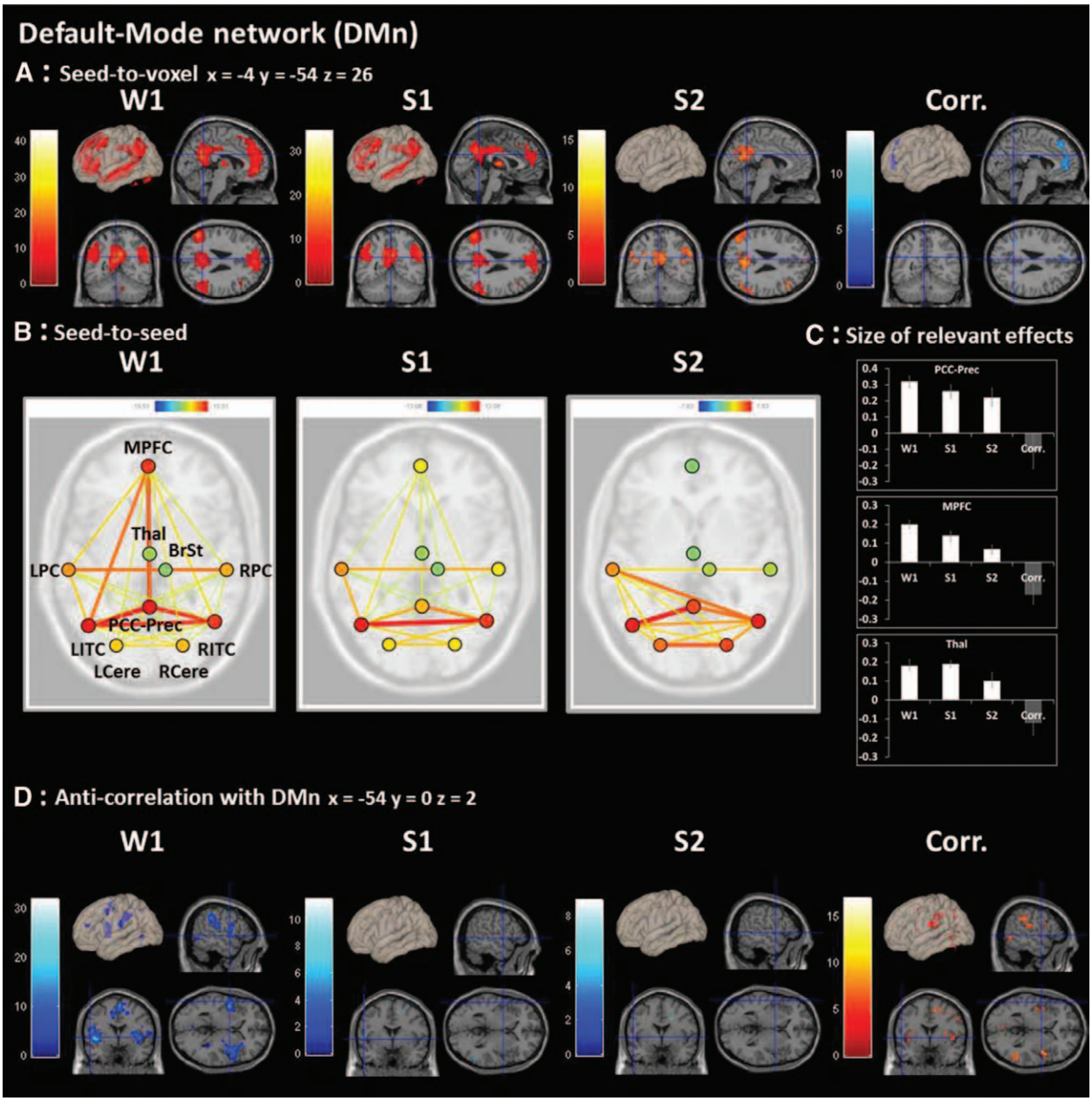

Fig. 2. (*A*) Connectivity maps according to the seed-to-voxel analysis in the default mode network (DMn) across experimental conditions, namely baseline (wake state [W1]), light sedation (S1), and deep sedation (S2). For display purposes, results are thresholded at an uncorrected $P < 0.001$ and are shown on slices of a canonical structural T1 magnetic resonance scan in the three planes, as well as on a three-dimensional representation of the cortical surface. *Color scales* correspond to T values of statistical parametric mapping group maps. *x*, *y*, and *z* indicate the Montreal Neurological Institute coordinates of the point located at the crossing of *blue lines*. Brain regions showing a significant negative correlation between increasing depth of ketamine sedation and connectivity with DMn are also shown (correlation between depth of ketamine sedation and connectivity of concerned region with remaining network [Corr.]), using a *blue scale*. (*B*) Connectivity maps obtained after seed-to-seed analysis and using predefined regions of interest (ROIs) of the DMn for the W1, S1, and S2. Those ROIs are represented by *color circles* projected on a canonical axial brain slice. The *lines* indicate connectivity, and their color and thickness vary as a function of the associated T value. A *color scale* of T values is defined for each image and appears on *top* of them. (*C*) Size β and 95% CI (*error bars*) of some of the relevant effects observed in ROIs of the DMn across experimental conditions (W1, S1, and S2) and for the correlation analysis. (*D*) Connectivity maps according to the seed-to-voxel analysis showing voxels that are anticorrelated with DMn across experimental conditions (W1, S1, and S2) and for the Corr. The coordinates of the point located at the crossing of *blue lines* are also indicated. *Color scale* has the same meaning as in (*A*). BrSt = brainstem; LCere/RCere = left and right cerebellum; LITC/RITC = left and right inferior temporal cortex; LPC/RPC = left and right lateral parietal cortices; MPFC = medial prefrontal cortex; PCC-Prec = posterior cingulate/precuneus; S1 = light sedation; S2 = deep sedation; Thal = thalamus.

The sixth (cluster 16) was located in the left dorsolateral prefrontal cortex and anterior prefrontal cortex and the seventh (cluster 18) in the left premotor cortex and primary motor cortex. These regions lost their anticorrelation with DMn during ketamine sedation, insofar as no significantly anticorrelated clusters were present during S1 and S2.

As illustrated in figure 2, increasing the depth of ketamine sedation was associated with an increase in connectivity with DMn in regions already identified as being anticorrelated with DMn during W1. This was the case for the above-cited clusters 7, 9, and 10. (Effect sizes are shown in Supplemental Digital Content 4, http://links.lww.com/ALN/B307; fig. 3.) In addition, increasing the depth of sedation was associated with an increase in connectivity with DMn in regions that were not anticorrelated with DMn during W1. Those regions were the cerebellum, parts of the left somatosensory association cortex, dorsal posterior cingulate cortex, parts of the right superior temporal gyrus, middle temporal gyrus, and fusiform gyrus (Supplemental Digital Content 4, http://links.lww.com/ALN/B307).

Left and Right Executive Control Networks

Cluster analysis during W1 (Supplemental Digital Content 3, http://links.lww.com/ALN/B306) confirmed significant connectivity between regions defined as pertaining to LECn and RECn. In addition, significant connectivity was identified between LECn and RECn. During the W1, anticorrelation between LECn or RECn and a region located in the posterior part of the cingulate cortex also showed up.

As illustrated in figure 3, increasing the depth of ketamine sedation had tenuous effect on connectivity within LECn and RECn. At S2, significant between region connectivity was still found within both networks. The only difference was an absence of significant connectivity between LECn and RECn at that deepest level of sedation. Correlation analysis did not reveal any significant relationship between the depth of sedation and connectivity within LECn or RECn. In contrast, two clusters centered in the right primary sensory cortex and right insula showed increased connectivity with RECn as a consequence of increasing the depth of sedation.

Salience Network

SALn was active during W1 (fig. 4), encompassing its 23 predefined seed regions. In addition, two clusters centered in the left and right cingulate cortices displayed significant anticorrelation with SALn during the same experimental condition.

S1 had few effects on SALn connectivity, in contrast to S2, where no cluster with significant SALn connectivity was identified. However, correlation analysis did not evidence any significant relationship between the depth of ketamine sedation and the decrease or increase in SALn connectivity.

Sensory and Motor Networks

In addition to its predefined seed regions, AUDn displayed large significant connectivity with multiple other cortical regions during W1 (fig. 5), including left and right insula, left and right prefrontal cortices, as well as regions involved in motor and somatosensory modalities. Significant anticorrelation was also identified between AUDn and a small region centered in the retrosplenial cingulate cortex.

VISn was evident during W1 (fig. 5). It displayed significant connectivity with somatosensory and motor cortex. Anticorrelation of this network with right supramarginal gyrus, superior temporal gyrus, insula, dorsal posterior cingulate cortex, and somatosensory association cortex was also evidenced.

Connectivity within SMn was also large during W1 (fig. 5) and extended to auditory and visual cortical regions. Two SMn anticorrelated clusters were also present during that experimental condition and located in the left and right retrosplenial cingulate cortices.

Increasing the depth of ketamine sedation had few effects on connectivity within those sensory and motor networks, insofar as most of their predefined seed regions were still showing significant connectivity during both S1 and S2, and no significant correlations between the depth of ketamine sedation and AUDn, VISn, or SMn connectivity were evidenced.

Discussion

In this study, we demonstrate that ketamine has specific, differential, and dose-dependent effects on connectivity within the most currently described RSNs (table 3). Although sharing some similarities with other hypnotic anesthetic agents, such as the effect on frontal-parietal connectivity, ketamine behaves differently in some aspects. Our findings refine our understanding of anesthesia mechanisms.

First, the frontal dissociation from the remaining DMn could be considered as a hallmark of unresponsiveness to command during anesthesia. Breakdown of connectivity within the DMn has already been demonstrated during alterations of consciousness induced by other hypnotic anesthetic agents, including propofol.[10] Particularly, disconnection of frontal-parietal connectivity has been shown to occur with propofol, sevoflurane, and ketamine in electrophysiologic studies.[6,23] In addition, ketamine does not modify connectivity within the DMn uniformly. Corticocortical interactions are preferential targets of ketamine, because thalamocortical connectivity remains relatively preserved, even at the deepest levels of sedation (fig. 2). This is in accordance with older and recent other findings[36] showing even increased thalamocortical connectivity by ketamine.[37] A preferential corticocortical effect and the preservation of RSNs' thalamocortical connectivity are also seen with propofol.[4,15] These could be arguments against the thalamic switch hypothesis, sustaining that the anesthetic state, as opposed to sedation, is driven by a thalamocortical disruption.[38] However, thalamocortical interactions are not

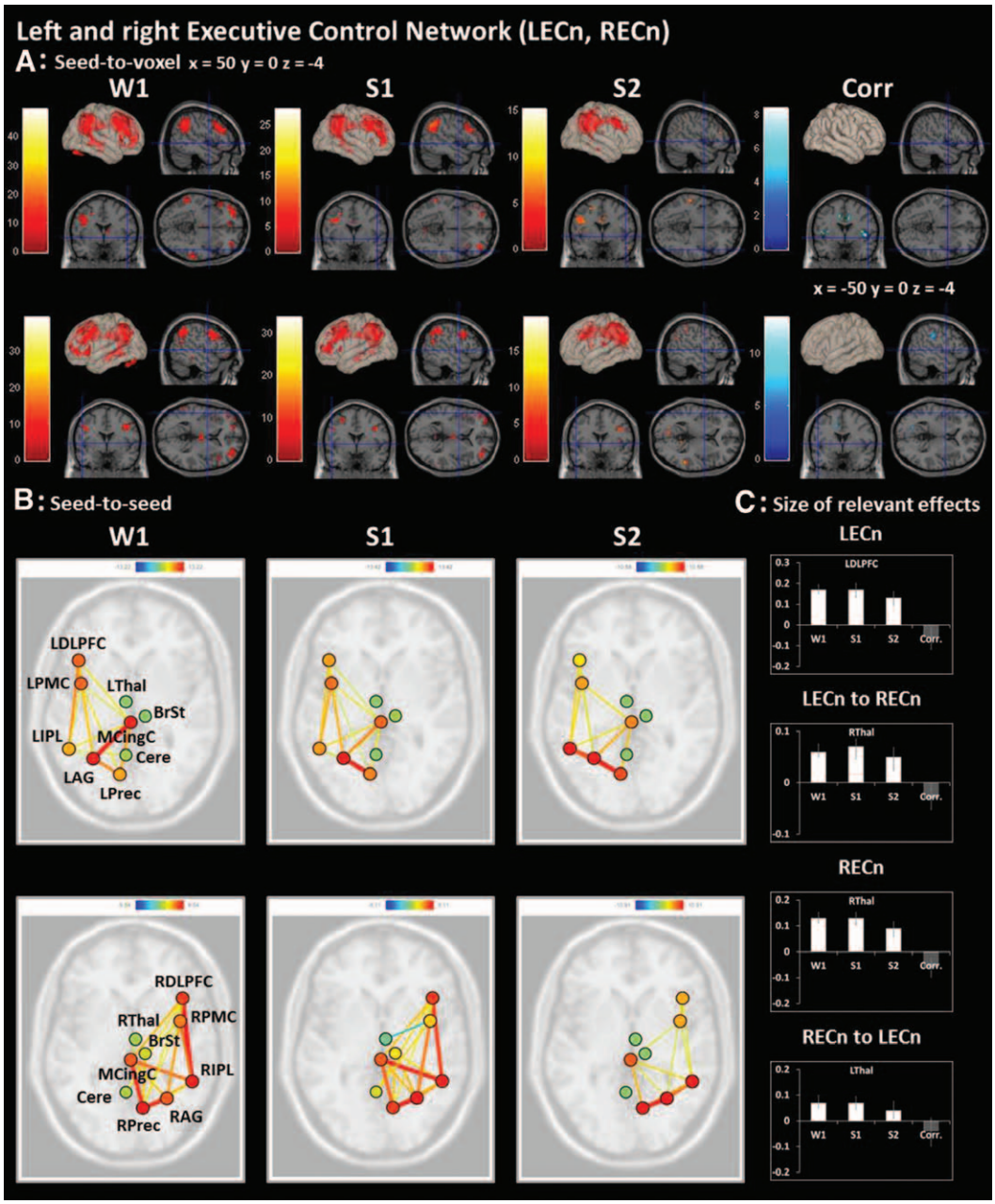

Fig. 3. (*A*) Connectivity maps according to the seed-to-voxel analysis in the left and right executive control networks (LECn and RECn) across experimental conditions, namely baseline (wake state [W1]), light sedation (S1), and deep sedation (S2). For display purposes, results are thresholded at an uncorrected $P < 0.001$ and are shown on slices of a canonical structural T1 magnetic resonance scan in the three planes, as well as on a three-dimensional representation of the cortical surface. *Color scales* correspond to T values of statistical parametric mapping group maps. *x*, *y*, and *z* indicate the Montreal Neurological Institute coordinates of the point located at the crossing of *blue lines*. Brain regions showing a significant negative correlation between the increasing depth of ketamine sedation and the connectivity with LECn or RECn are also shown (correlation between depth of ketamine sedation and connectivity of concerned region with remaining network [Corr.]), using a *blue scale*. (*B*) Connectivity maps obtained after seed-to-seed analysis and using predefined regions of interest (ROIs) of the LECn and RECn for W1, S1, and S2. Those ROIs are represented by *color circles* projected on a canonical axial brain slice. The *lines* indicate connectivity, and their color and thickness vary as a function of the associated T value. A *color scale* of T values is defined for each image and appears on *top* of them. (*C*) Size β and 95% CI (*error bars*) of some of the relevant effects observed in ROIs of the LECn and RECn across experimental conditions (W1, S1, and S2) and for the correlation analysis. Effect sizes are shown for connectivity between those ROIs and ipsilateral (LECn and RECn) or contralateral (LECn to RECn, RECn to LECn) executive control network. BrSt = brainstem; Cere = cerebellum; LAG/RAG = left and right angular gyrus; LDLPFC/RDLPFC = left and right dorsolateral prefrontal cortices; LIPL/RIPL = left and right inferior parietal lobules; LPMC/RPMC = left and right premotor cortices; LPrec/RPrec = left and right precuneus; LThal/RThal = left and right thalamus; MCingC = midcingulate cortex.

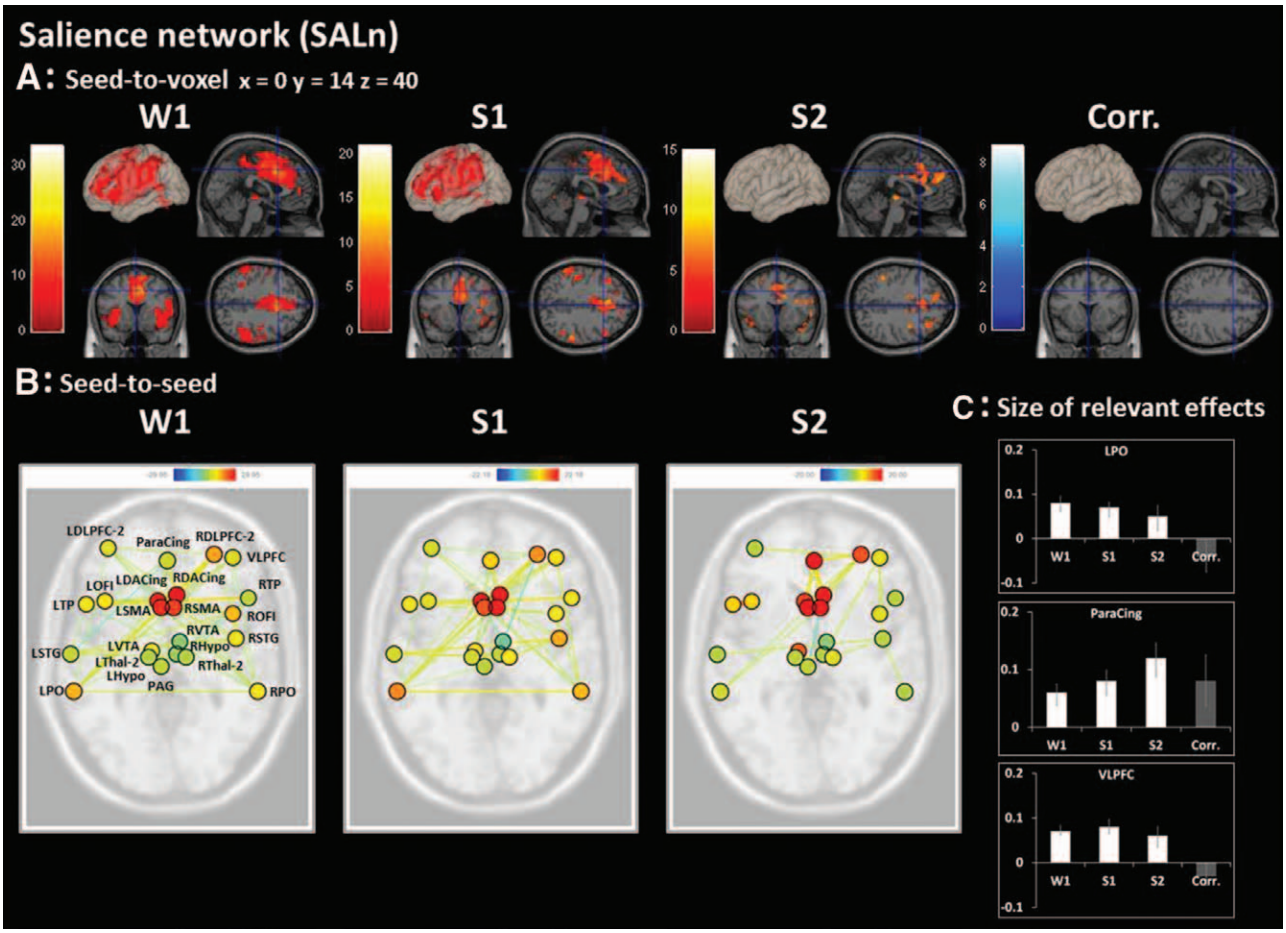

Fig. 4. (*A*) Connectivity maps according to the seed-to-voxel analysis in the salience network (SALn) across experimental conditions, namely baseline (wake state [W1]), light sedation (S1), and deep sedation (S2). For display purposes, results are thresholded at an uncorrected $P < 0.001$ and are shown on slices of a canonical structural T1 magnetic resonance scan in the three planes, as well as on a three-dimensional representation of the cortical surface. *Color scales* correspond to T values of statistical parametric mapping group maps. *x*, *y*, and *z* indicate the Montreal Neurological Institute coordinates of the point located at the crossing of *blue lines*. Correlation analysis did not disclose any brain regions showing a significant correlation between increasing the depth of ketamine sedation and the connectivity with SALn (correlation between depth of ketamine sedation and connectivity of concerned region with remaining network [Corr.]). (*B*) Connectivity maps obtained after seed-to-seed analysis and using predefined regions of interest (ROIs) of the SALn for the W1, S1, and S2. Those ROIs are represented by *color circles* projected on a canonical axial brain slice. The *lines* indicate connectivity, and their color and thickness vary as a function of the associated T value. A *color scale* of T values is defined for each image and appears on *top* of them. (*C*) Size β and 95% CI (*error bars*) of some of the relevant effects observed in ROIs of the SALn across experimental conditions (W1, S1, and S2) and for the correlation analysis (Corr.). LDACing/RDACing = left and right dorsal anterior cingulate; LDLPFC-2/RDLPFC-2 = left and right dorsolateral prefrontal cortices; Lhypo/Rhypo = left and right hypothalamus; LOFI/ROFI = left and right orbital frontoinsula; LPO/RPO = left and right parietal operculum; LSMA/RSMA = left and right supplementary motor areas; LSTG/RSTG = left and right superior temporal gyrus; Lthal-2/Rthal-2 = left and right thalamus; LTP/RTP = left and right temporal poles; LVTA/RVTA = left and right ventral tegmental areas; PAG = periaqueductal gray; ParaCing = paracingulate; VLPFC = ventrolateral prefrontal cortex.

limited to those involved in RSNs. Other less specific thalamocortical interactions play a role in cortical arousal.[9] Our observations in RSNs could be the consequences of an inhibition of such interactions, and the DMn disruption could simply be the witness of interoceptive processes alteration. Determining the precise role of thalamocortical interactions during ketamine anesthesia would require dedicated analyses, using specific techniques targeting the thalamus.[15]

Second, ketamine reorganizes DMn connectivity toward newer cortical regions (fig. 2). The ability of ketamine to reorganize brain networks has already been shown by others[20,21] and is already evident at lower doses than those of this study. This effect may be related to ketamine-induced psychotomimesis. A systematic comparison with changes observed in those two other studies is not straightforward, insofar as networks were differently defined, and ketamine mode of administration and doses were not the same. However, ketamine evidently reorganizes brain connectivity with the regions that are involved in interoceptive and exteroceptive sensory processing. The link between the observed reorganization and psychedelic dreaming

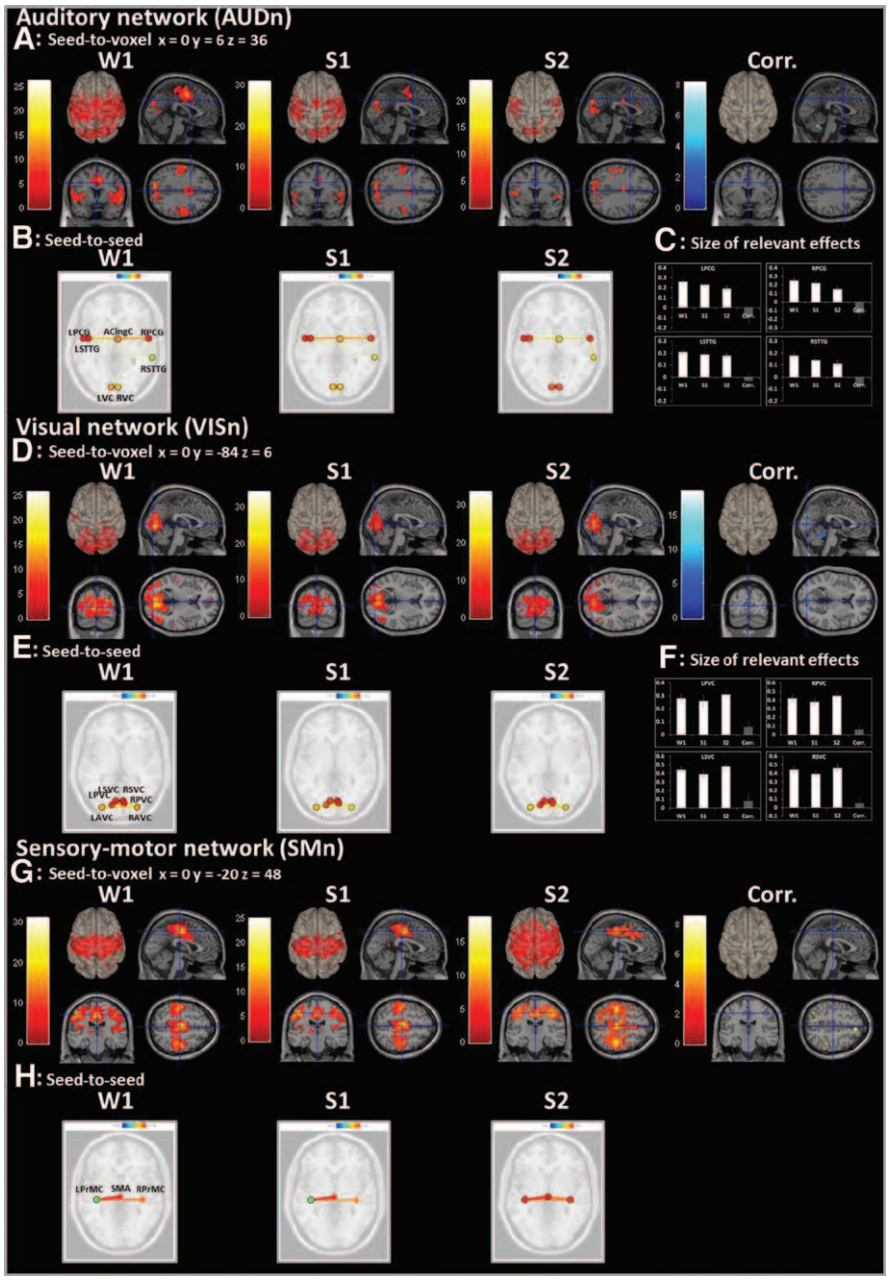

Fig. 5. Connectivity maps according to the seed-to-voxel analysis in the auditroy (AUDn) (*A*), visual (VISn) (*D*), and sensorimotor (SMn) (*G*) networks across experimental conditions, namely baseline (wake state [W1]), light sedation (S1), and deep sedation (S2). For display purposes, results are thresholded at an uncorrected $P < 0.001$ and are shown on slices of a canonical structural T1 magnetic resonance scan in the three planes, as well as on a three-dimensional representation of the cortical surface. *Color scales* correspond to T values of statistical parametric mapping group maps. *x*, *y*, and *z* indicate the Montreal Neurological Institute coordinates of the point located at the crossing of *blue lines*. Correlation analysis did not evidence any brain regions showing a significant correlation between the increasing depth of ketamine sedation and the connectivity with concerned networks (correlation between depth of ketamine sedation and connectivity of concerned region with remaining network [Corr.]). Connectivity maps were obtained after seed-to-seed analysis and using predefined regions of interest (ROIs) of the AUDn (*B*), VISn (*E*), and SMn (*H*) for W1, S1, and S2. Those ROIs are represented by *color circles* projected on a canonical axial brain slice. The lines indicate connectivity, and their color and thickness vary as a function of the associated T value. A *color scale* of T values is defined for each image and appears on *top* of them. Size β and 95% CI (*error bars*) of some of the relevant effects observed in ROIs of the AUDn (*C*) and VISn (*F*) across experimental conditions (W1, S1, and S2) and for the correlation analysis (Corr.) are also shown. ACingC = anterior cingulate cortex; LAVC/RAVC = left and right associative visual cortices; LPCG/RPCG = left and right precentral gyrus; LPrMC/RPrMC = left and right primary motor cortices; LPVC/RPVC = left and right primary visual cortices; LSTTG/RSTTG = left and right superior transverse temporal gyrus; LSVC/RSVC = left and right secondary visual cortices; LVC/RVC = left and right visual cortices; S1 = light sedation; S2 = deep sedation; SMA = supplementary motor area.

Table 3. Summary of Salient Findings regarding Connectivity in Studied Networks at Different Depths of Ketamine Sedation

Network	Effects on Connectivity
DMn	Breakdown of DMn by ketamine, discreet during light sedation, more pronounced during loss of responsiveness The main disconnection is frontal Decreased thalamic connectivity during ketamine-induced loss of responsiveness, but still present Ketamine increases connectivity between DMn and several other brain regions Anticorrelation with DMn is markedly reduced by ketamine, even during light sedation
LECn an	Tenuous effect of ketamine on LECn and RECn
RECn	Ketamine increases connectivity between RECn and right primary sensory cortex Ketamine increases connectivity between RECn and right insula Absence of significant interactions between LECn and RECn during ketamine-induced loss of responsiveness to command
SALn	Few changes during light ketamine sedation Breakdown during ketamine-induced loss of responsiveness to command Heterogeneous alteration within the network
AUDn	No remarkable effect
VISn	No cross modal interaction inhibition
SMn	

AUDn = auditory network; DMn = default mode network; LECn = left executive control network; RECn = right executive control network; SALn = salience network; SMn = sensorimotor network; VISn = visual network.

is not evident, because the sedation stage where they occurred in our study is not known. Doses of ketamine producing unresponsiveness are associated with disconnected consciousness, corresponding to isolation from the environment with psychedelic dreaming. This state is characterized by a complex spatiotemporal pattern of cortical activity, as opposed to propofol.[39] In addition, connectivity within LECn and RECn is remarkably preserved during ketamine-induced loss of responsiveness, contrarily to DMn. This finding contrasts with the effects of propofol, which switches them off.[10] The functional significance of ECn preservation is not known. One hypothesis could be a preserved influence of environmental input on brain function during ketamine sedation, although this external information could not reach a normal conscious field. The conjunction with SALn nonuniform breakdown (fig. 4) could generate inadequate processing of external information and inability to discern salience of external input. Of note, the nonuniform breakdown of SALn is probably the reason why we were not able to evidence any significant relationship between the depth of ketamine sedation and SALn connectivity. Apart from those effects, functional anticorrelation with DMn is affected by ketamine, already at low concentrations. This is similar to propofol[10] and could be, along with the frontal-parietal connectivity breakdown, a common feature of anesthesia-induced alteration of consciousness. Such modification of DMn activity alternation with other networks probably reflects the inability to switch between external and internal awareness[16] and could participate in the installation of a disconnected consciousness state.

Finally, ketamine very tenuously influences connectivity within sensory and motor networks. Although preserving sensory network functional connectivity, ketamine may still alter sensory information transfer, as shown in a recent primate study demonstrating a block of that transfer at the corticocortical rather than the thalamocortical level during ketamine sedation.[40] Cross-modal interactions between auditory and VISns are also preserved. This is, in addition to ECn preservation and cortical connectivity reorganization, a difference with propofol sedation, where cross-modal interaction is impeded.[10] Those differences between ketamine and propofol can be at the origin of the different clinical patterns of sedation, namely disconnected consciousness during ketamine sedation and loss of mental content with disconnection from the environment during propofol sedation. Preservation of SMn connectivity during ketamine sedation is in accordance with the frequent observation of apparently nonpurposeful movements at that time.

We would like to mention, however, that our sample size is relatively small, and we may have missed some significant effects on resting-state network connectivity. We have excluded 6 of 14 subjects from analysis, mainly because of excessive agitation inside the scanner and the impossibility of acquiring complete data sets. As a consequence, important effects of ketamine may have been missed and particularly those linked to agitation. In addition, these difficulties were a strong limitation to recruiting more of them, for ethical reasons. Hence, we can be confident in the observed significant effects, but less in negative results. A sample size of 20 subjects is generally considered optimal in studies such as this one,[41] but ours is in the range of most published fMRI studies investigating the effect of sedation, namely between 7 and 19.[10] In addition, we used a random-effects approach at the group level, which allows confidence that our results are representative of the sampled population. Regarding the absence of effect, results were concordant when comparing S2-W1 subtraction analyses (not reported here), where a FDR-corrected *P* threshold of 0.05 was chosen, and corresponding correlation analyses, where a more liberal uncorrected *P* threshold of 0.001 was used. This indicates that, even when being more liberal, no effect emerged.

Our results might have been biased by the choice of a multiple-seed ROI approach. Studies using this kind of method now accumulate, demonstrating an acceptable degree of reproducibility. The demonstration of resting-state connectivity modulation by anesthesia reinforces the conviction that resting-state networks effectively represent functional correlates of consciousness.[42] A multiple-seed approach for each network additionally

limits the risk of selection bias,[43] insofar as it includes well-identified nodes of each network.[44] It ensures proper network characterization. Further analysis of our data by a convergent functional connectivity analysis method, or independent component analysis, will confirm having not missed network nodes through the use of a conventional ROI-driven analysis.[45]

During the experiment, we were not able to control for closing or opening of the volunteers' eyes. All volunteers had their eyes closed during the baseline condition (W1), but did not obey to the instruction of keeping them closed once having received ketamine. This may have influenced brain activity in an uncontrolled way, but probably to a small extent, because data acquisition occurred in a dark room.

The order of experimental conditions was not randomized, for the reason that ketamine has long recovery times.[46] Randomizing conditions would have unduly prolonged time spent in the scanner for the volunteer, without certainty regarding the ability to obtain all desired sedation stages because of agitation.

Last, some physiologic variations may have influenced our results, including arterial carbon dioxide, heart rate, and blood pressure variations. Ketamine is known to increase CBF in excess of metabolic needs[47] and may therefore perturb CBF regulation, independently from cerebral activity. But some flow metabolism coupling persists,[47] and resting-state fMRI studies look at between-region statistical dependencies in BOLD fluctuation, not at regional variation in CBF *per se*. Regarding heart rate and blood pressure, which substantially increased with the depth of sedation, they unlikely had influence on our results. Indeed, ketamine is known to have few effects on pressure-flow cerebrovascular autoregulation, at least in animals.[48] Carbon dioxide arterial concentration has also had few effects on our results, because it did not vary significantly.

Conclusions

On the basis of the differential effects on functional connectivity patterns, we confirm the perspective that ketamine is a unique anesthetic drug. However, ketamine-induced unresponsiveness shares common features with GABAergic drugs, including breakdown of frontal-parietal connectivity and DMn anticorrelation. This is a supplementary argument to consider the presence of such connectivity and anticorrelation as witnesses of the presence of normal conscious thoughts. Aside from these common effects, the differential effects of hypnotic anesthetic agents on those networks probably account for their ability to modulate mental content and connectedness to the environment differently. Ketamine seems to preserve subcortical input to the cortex, as well as sensory and motor processing. The alteration of higher-order integration networks, such as the DMn, its anticorrelation with other networks, and SALn, are responsible for mental content perturbation during ketamine sedation.

Research Support

Supported by the Society for Anesthesia and Resuscitation of Belgium (Brussels, Belgium), the Belgian National Funds for Scientific Research (Brussels, Belgium), where Dr. Demertzi is a postdoctoral and Dr. Laureys is a research director, the European Commission (Brussels, Belgium), the James McDonnell Foundation (Saint Louis, Missouri), the European Space Agency (Brussels, Belgium), the Mind Science Foundation (San Antonio, Texas), the French Speaking Community Concerted Research Action (ARC - 06/11 – 340, Brussels, Belgium), the Public Utility Foundation "Université Européenne du Travail" (Brussels, Belgium), "Fondazione Europea di Ricerca Biomedica" (Milan, Italy), and the University and University Hospital of Liege (Liege, Belgium).

Competing Interests

The authors declare no competing interests.

Correspondence

Address correspondence to Dr. Bonhomme: University Department of Anesthesia and Intensive Care Medicine, CHR Citadelle, Bd du 12eme de Ligne, 1, 4000 Liege, Belgium. vincent.bonhomme@chu.ulg.ac.be. This article may be accessed for personal use at no charge through the Journal Web site, www.anesthesiology.org.

References

1. Bonhomme V, Boveroux P, Brichant JF, Laureys S, Boly M: Neural correlates of consciousness during general anesthesia using functional magnetic resonance imaging (fMRI). Arch Ital Biol 2012; 150:155–63
2. Pattinson KT: Functional magnetic resonance imaging in anaesthesia research. Br J Anaesth 2013; 111:872–6
3. Friston K, Moran R, Seth AK: Analysing connectivity with Granger causality and dynamic causal modelling. Curr Opin Neurobiol 2013; 23:172–8
4. Guldenmund P, Demertzi A, Boveroux P, Boly M, Vanhaudenhuyse A, Bruno MA, Gosseries O, Noirhomme Q, Brichant JF, Bonhomme V, Laureys S, Soddu A: Thalamus, brainstem and salience network connectivity changes during propofol-induced sedation and unconsciousness. Brain Connect 2013; 3:273–85
5. Lee H, Mashour GA, Noh GJ, Kim S, Lee U: Reconfiguration of network hub structure after propofol-induced unconsciousness. Anesthesiology 2013; 119:1347–59
6. Ku SW, Lee U, Noh GJ, Jun IG, Mashour GA: Preferential inhibition of frontal-to-parietal feedback connectivity is a neurophysiologic correlate of general anesthesia in surgical patients. PLoS One 2011; 6:e25155
7. Amico E, Gomez F, Di Perri C, Vanhaudenhuyse A, Lesenfants D, Boveroux P, Bonhomme V, Brichant JF, Marinazzo D, Laureys S: Posterior cingulate cortex-related co-activation patterns: A resting state FMRI study in propofol-induced loss of consciousness. PLoS One 2014; 9:e100012
8. Jordan D, Ilg R, Riedl V, Schorer A, Grimberg S, Neufang S, Omerovic A, Berger S, Untergehrer G, Preibisch C, Schulz E, Schuster T, Schröter M, Spoormaker V, Zimmer C, Hemmer B, Wohlschläger A, Kochs EF, Schneider G: Simultaneous electroencephalographic and functional magnetic resonance imaging indicate impaired cortical top-down processing in association with anesthetic-induced unconsciousness. Anesthesiology 2013; 119:1031–42
9. Hudetz AG: General anesthesia and human brain connectivity. Brain Connect 2012; 2:291–302
10. Boveroux P, Vanhaudenhuyse A, Bruno MA, Noirhomme Q, Lauwick S, Luxen A, Degueldre C, Plenevaux A, Schnakers C, Phillips C, Brichant JF, Bonhomme V, Maquet P, Greicius MD, Laureys S, Boly M: Breakdown of within- and between-network resting state functional magnetic resonance imaging

connectivity during propofol-induced loss of consciousness. Anesthesiology 2010; 113:1038–53
11. Buckner RL, Andrews-Hanna JR, Schacter DL: The brain's default network: Anatomy, function, and relevance to disease. Ann NY Acad Sci 2008; 1124:1–38
12. Damoiseaux JS, Rombouts SA, Barkhof F, Scheltens P, Stam CJ, Smith SM, Beckmann CF: Consistent resting-state networks across healthy subjects. Proc Natl Acad Sci USA 2006; 103:13848–53
13. Laird AR, Fox PM, Eickhoff SB, Turner JA, Ray KL, McKay DR, Glahn DC, Beckmann CF, Smith SM, Fox PT: Behavioral interpretations of intrinsic connectivity networks. J Cogn Neurosci 2011; 23:4022–37
14. Shackman AJ, Salomons TV, Slagter HA, Fox AS, Winter JJ, Davidson RJ: The integration of negative affect, pain and cognitive control in the cingulate cortex. Nat Rev Neurosci 2011; 12:154–67
15. Boly M, Moran R, Murphy M, Boveroux P, Bruno MA, Noirhomme Q, Ledoux D, Bonhomme V, Brichant JF, Tononi G, Laureys S, Friston K: Connectivity changes underlying spectral EEG changes during propofol-induced loss of consciousness. J Neurosci 2012; 32:7082–90
16. Vanhaudenhuyse A, Demertzi A, Schabus M, Noirhomme Q, Bredart S, Boly M, Phillips C, Soddu A, Luxen A, Moonen G, Laureys S: Two distinct neuronal networks mediate the awareness of environment and of self. J Cogn Neurosci 2011; 23:570–8
17. Sleigh J, Harvey M, Voss L, Denny B: Ketamine—More mechanisms of action than just NMDA blockade. Trends Anaesth Crit Care 2014; 4:76–81
18. Liao Y, Tang J, Fornito A, Liu T, Chen X, Chen H, Xiang X, Wang X, Hao W: Alterations in regional homogeneity of resting-state brain activity in ketamine addicts. Neurosci Lett 2012; 522:36–40
19. Scheidegger M, Walter M, Lehmann M, Metzger C, Grimm S, Boeker H, Boesiger P, Henning A, Seifritz E: Ketamine decreases resting state functional network connectivity in healthy subjects: Implications for antidepressant drug action. PLoS One 2012; 7:e44799
20. Niesters M, Khalili-Mahani N, Martini C, Aarts L, van Gerven J, van Buchem MA, Dahan A, Rombouts S: Effect of subanesthetic ketamine on intrinsic functional brain connectivity: A placebo-controlled functional magnetic resonance imaging study in healthy male volunteers. Anesthesiology 2012; 117:868–77
21. Driesen NR, McCarthy G, Bhagwagar Z, Bloch M, Calhoun V, D'Souza DC, Gueorguieva R, He G, Ramachandran R, Suckow RF, Anticevic A, Morgan PT, Krystal JH: Relationship of resting brain hyperconnectivity and schizophrenia-like symptoms produced by the NMDA receptor antagonist ketamine in humans. Mol Psychiatry 2013; 18:1199–204
22. Driesen NR, McCarthy G, Bhagwagar Z, Bloch MH, Calhoun VD, D'Souza DC, Gueorguieva R, He G, Leung HC, Ramani R, Anticevic A, Suckow RF, Morgan PT, Krystal JH: The impact of NMDA receptor blockade on human working memory-related prefrontal function and connectivity. Neuropsychopharmacology 2013; 38:2613–22
23. Lee U, Ku S, Noh G, Baek S, Choi B, Mashour GA: Disruption of frontal-parietal communication by ketamine, propofol, and sevoflurane. Anesthesiology 2013; 118:1264–75
24. Blain-Moraes S, Lee U, Ku S, Noh G, Mashour GA: Electroencephalographic effects of ketamine on power, cross-frequency coupling, and connectivity in the alpha bandwidth. Front Syst Neurosci 2014; 8:114
25. Domino EF, Zsigmond EK, Domino LE, Domino KE, Kothary SP, Domino SE: Plasma levels of ketamine and two of its metabolites in surgical patients using a gas chromatographic mass fragmentographic assay. Anesth Analg 1982; 61:87–92
26. Absalom AR, Lee M, Menon DK, Sharar SR, De Smet T, Halliday J, Ogden M, Corlett P, Honey GD, Fletcher PC: Predictive performance of the Domino, Hijazi, and Clements models during low-dose target-controlled ketamine infusions in healthy volunteers. Br J Anaesth 2007; 98:615–23
27. Ramsay MA, Savege TM, Simpson BR, Goodwin R: Controlled sedation with alphaxalone-alphadolone. Br Med J 1974; 2:656–9
28. Malviya S, Voepel-Lewis T, Tait AR, Merkel S, Tremper K, Naughton N: Depth of sedation in children undergoing computed tomography: Validity and reliability of the University of Michigan Sedation Scale (UMSS). Br J Anaesth 2002; 88:241–5
29. Fox MD, Snyder AZ, Vincent JL, Corbetta M, Van Essen DC, Raichle ME: The human brain is intrinsically organized into dynamic, anticorrelated functional networks. Proc Natl Acad Sci USA 2005; 102:9673–8
30. Raichle ME: The restless brain. Brain Connect 2011; 1:3–12
31. Fair DA, Cohen AL, Power JD, Dosenbach NU, Church JA, Miezin FM, Schlaggar BL, Petersen SE: Functional brain networks develop from a "local to distributed" organization. PLoS Comput Biol 2009; 5:e1000381
32. Seeley WW, Menon V, Schatzberg AF, Keller J, Glover GH, Kenna H, Reiss AL, Greicius MD: Dissociable intrinsic connectivity networks for salience processing and executive control. J Neurosci 2007; 27:2349–56
33. Maudoux A, Lefebvre P, Cabay JE, Demertzi A, Vanhaudenhuyse A, Laureys S, Soddu A: Auditory resting-state network connectivity in tinnitus: A functional MRI study. PLoS One 2012; 7:e36222
34. De Luca M, Beckmann CF, De Stefano N, Matthews PM, Smith SM: fMRI resting state networks define distinct modes of long-distance interactions in the human brain. Neuroimage 2006; 29:1359–67
35. Demertzi A, Antonopoulos G, Heine L, Voss HU, Crone JS, de Los Angeles C, Bahri MA, Di Perri C, Vanhaudenhuyse A, Charland-Verville V, Kronbichler M, Trinka E, Phillips C, Gomez F, Tshibanda L, Soddu A, Schiff ND, Whitfield-Gabrieli S, Laureys S: Intrinsic functional connectivity differentiates minimally conscious from unresponsive patients. Brain 2015; 138(pt 9):2619–31
36. Ferrer-Allado T, Brechner VL, Dymond A, Cozen H, Crandall P: Ketamine-induced electroconvulsive phenomena in the human limbic and thalamic regions. Anesthesiology 1973; 38:333–44
37. Höflich A, Hahn A, Küblböck M, Kranz GS, Vanicek T, Windischberger C, Saria A, Kasper S, Winkler D, Lanzenberger R: Ketamine-induced modulation of the thalamo-cortical network in healthy volunteers as a model for schizophrenia. Int J Neuropsychopharmacol 2015; 18
38. Alkire MT, Haier RJ, Fallon JH: Toward a unified theory of narcosis: Brain imaging evidence for a thalamocortical switch as the neurophysiologic basis of anesthetic-induced unconsciousness. Conscious Cogn 2000; 9:370–86
39. Sarasso S, Boly M, Napolitani M, Gosseries O, Charland-Verville V, Casarotto S, Rosanova M, Casali AG, Brichant JF, Boveroux P, Rex S, Tononi G, Laureys S, Massimini M: Consciousness and complexity during unresponsiveness induced by propofol, xenon, and ketamine. Curr Biol 2015; 25:3099–105
40. Schroeder KE, Irwin ZT, Gaidica M, Bentley JN, Patil PG, Mashour GA, Chestek CA: Disruption of corticocortical information transfer during ketamine anesthesia in the primate brain. Neuroimage 2016; 134:459–65
41. Thirion B, Pinel P, Mériaux S, Roche A, Dehaene S, Poline JB: Analysis of a large fMRI cohort: Statistical and methodological issues for group analyses. Neuroimage 2007; 35:105–20
42. Barttfeld P, Uhrig L, Sitt JD, Sigman M, Jarraya B, Dehaene S: Signature of consciousness in the dynamics of resting-state brain activity. Proc Natl Acad Sci USA 2015; 112:887–92
43. Smith DV, Utevsky AV, Bland AR, Clement N, Clithero JA, Harsch AE, McKell Carter R, Huettel SA: Characterizing individual differences in functional connectivity using dual-regression and seed-based approaches. Neuroimage 2014; 95:1–12
44. Cole DM, Smith SM, Beckmann CF: Advances and pitfalls in the analysis and interpretation of resting-state FMRI data. Front Syst Neurosci 2010; 4:8

45. Seeley WW, Menon V, Schatzberg AF, Keller J, Glover GH, Kenna H, Reiss AL, Greicius MD: Dissociable intrinsic connectivity networks for salience processing and executive control. J Neurosci 2007; 27:2349–56

46. Parashchanka A, Schelfout S, Coppens M: Role of novel drugs in sedation outside the operating room: Dexmedetomidine, ketamine and remifentanil. Curr Opin Anaesthesiol 2014; 27:442–7

47. Långsjö JW, Maksimow A, Salmi E, Kaisti K, Aalto S, Oikonen V, Hinkka S, Aantaa R, Sipilä H, Viljanen T, Parkkola R, Scheinin H: S-ketamine anesthesia increases cerebral blood flow in excess of the metabolic needs in humans. Anesthesiology 2005; 103:258–68

48. Schmidt A, Ryding E, Akeson J: Racemic ketamine does not abolish cerebrovascular autoregulation in the pig. Acta Anaesthesiol Scand 2003; 47:569–75

ANESTHESIOLOGY REFLECTIONS FROM THE WOOD LIBRARY-MUSEUM

From Baking Up Nitrous Oxide to Making the Home Thermostat: The Heat Regulators of Alfred W. Sprague

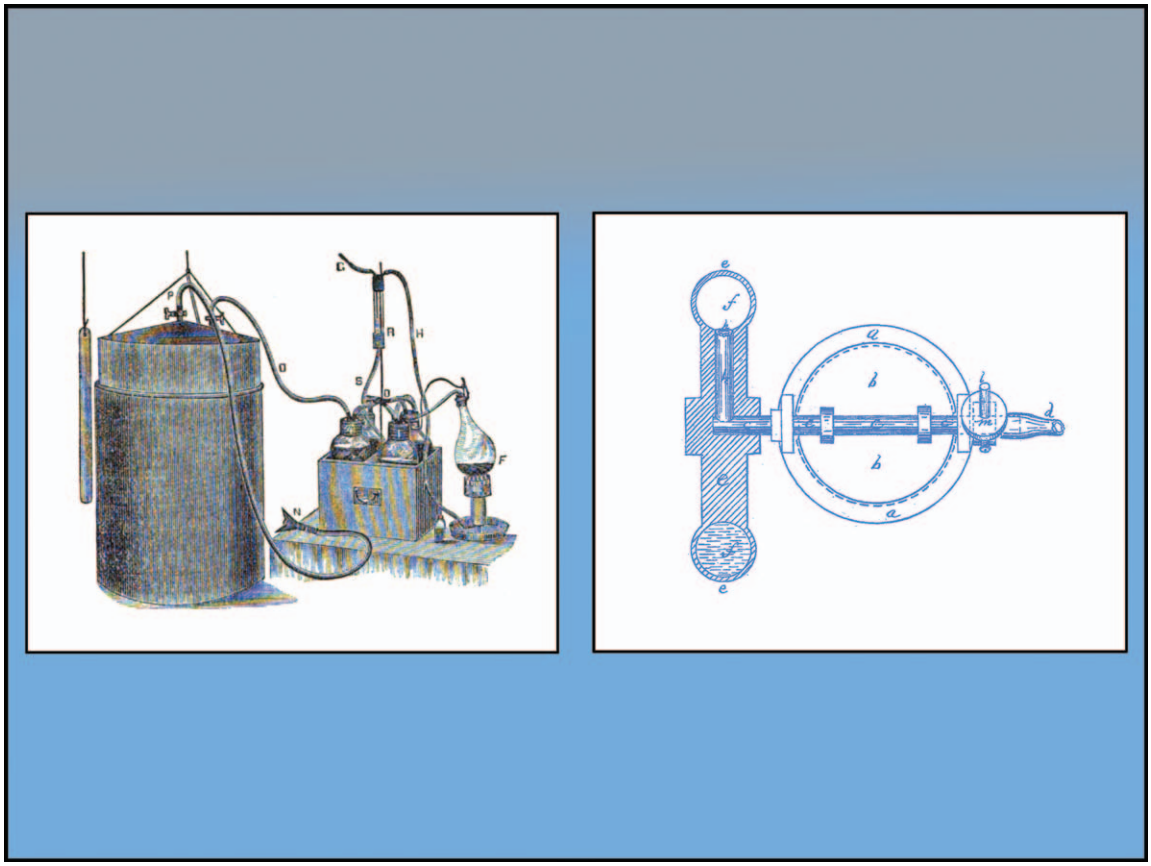

The most popular early method for generating nitrous oxide in the dental or medical office (or for recreational demonstrations) was to bake solid ammonium nitrate. Heated gently past its ~170°C melting point but less than 240°C, the ammonium nitrate decomposed into nitrous oxide and water. Heating to higher temperatures could lead to explosive detonation, yielding water and free nitrogen and oxygen gas. In June of 1866, a teacher of natural philosophy, Alfred W. Sprague, was granted a U.S. patent for his "Improved Apparatus for Generating and Washing Gases for Inhalation." His invention (*left*) was designed, first, to regulate "the heat where a given and uniform temperature is required; and, secondly, to produce a means for thoroughly washing and purifying the gas as it passes through the water." In April of 1873, Sprague shared a patent (*right*) for an "Improvement in Automatic Draft-Regulators for Stoves and Furnaces." So the same man who regulated heat for safely producing laughing gas later developed a safe means for burning natural gas. (Copyright © the American Society of Anesthesiologists' Wood Library-Museum of Anesthesiology.)

George S. Bause, M.D., M.P.H., Honorary Curator, ASA's Wood Library-Museum of Anesthesiology, Schaumburg, Illinois, and Clinical Associate Professor, Case Western Reserve University, Cleveland, Ohio. UJYC@aol.com.